Journal of Drug Delivery Science and Technology 96 (2024) 105723

Contents lists available at ScienceDirect

Journal of Drug Delivery Science and Technology

journal homepage: www.elsevier.com/locate/jddst

Sequential release of drugs from dual-delivery plasmonic nanogels containing lipid-gated mesoporous silica-coated gold nanorods

Filipa Costa-e-Sá [a,b], María Comís-Tuche [c], Carlos Spuch [c], Elisabete M.S. Castanheira [a,b], Sérgio R.S. Veloso [a,b,*]

[a] Physics Centre of Minho and Porto Universities (CF-UM-UP), University of Minho, Campus de Gualtar, 4710-057, Braga, Portugal
[b] LaPMET Associate Laboratory, University of Minho, Campus de Gualtar, 4710-057, Braga, Portugal
[c] Translational Neuroscience Research Group, Galicia Sur Health Research Institute (IIS-Galicia Sur), SERGAS-UVIGO, CIBERSAM, Vigo, Spain

ARTICLE INFO

Keywords:
Photothermia
Nanogels
Mesoporous nanoparticles
Gold nanorods
Sequential delivery

ABSTRACT

Nanosystems that enable the sequential delivery of various drugs with different targets are desired for improved cancer therapy. However, current strategies are mainly dependent on the tumour microenvironment, such as low pH or enzyme-triggered release. In this work, a nanosystem design strategy for near infrared (NIR) light-triggered sequential delivery based on lipid-gated mesoporous silica-coated gold nanorods and chitosan/alginate nanogels was developed. The mesoporous silica particles (99 ± 11 nm) were loaded with methotrexate, and further coated with a thermoresponsive phospholipid bilayer that works as gatekeeper. These particles were then incorporated in a chitosan/alginate nanogel matrix containing doxorubicin. The plasmonic nanogels exhbited high loading efficiencies of ~90 % and ~85 for methotrexate and doxorubicin, respectively. Notably, this system displayed average hydrodynamic diameters near 300 nm, low polidispersity, highly negative zeta potential (~−30 mV), and a sustained release of both drugs under acidic and neutral conditions. Upon NIR laser irradiation, an enhanced release of both drugs was observed, with doxorubicin exhibiting a faster release rate than methotrexate under acidic conditions. This design strategy of NIR-triggered sequential delivery holds promise for different drug combinations against multiple targets in tumour microenvironment in the field of multimodal cancer therapy.

1. Introduction

Cancer is among the principal causes of death worldwide, causing about 10 million deaths in 2020, according to the World Health Organization (WHO) [1]. Systemic chemotherapy lacks of targeting and selectivity leading to serious side effects and limited antitumor efficacy [2]. The single-drug treatment efficacy is usually poor, while the combination therapy of different drugs has shown improved therapeutic outcomes [3–5]. The co-delivery by nanocarriers further enhance the efficacy of combination therapy with the improved targeting to the tumor site [4–6]. Vyxeos, a liposome formulation for co-delivery of daunorubicin and cytarabine was approved by FDA, extending the overall survival of patients diagnosed with secondary acute myeloid leukemia (sAML) to 9.6 months compared to the 5.9 month for free drug combination [7]. Several strategies have been described to make use of the tumor microenvironment, which include enzyme-, pH- and redox-triggered systems [8–11]. These systems commonly explore the high concentration of proteases [12], reactive oxygen species [13], and acidic pH of tumor microenvironment [14–17]. However, the degradation of the nanocarriers by these stimuli is a time-consuming process [18], and the intrinsic heterogeneity of tumors causes problems with the basic mechanism of these systems [14]. Instead, temperature-sensitive systems can provide improved control over drug release [14,19–26].

Doxorubicin (DOX) and methotrexate (MTX) are widely used chemotherapeutic agents in numerous cancers. DOX is an anthracycline known to inhibit topoisomerase II and disrupt gene expression through intercalation into DNA [27]. However, its use is limited by dose-dependent side effects, such as cardiotoxicity [28]. MTX is a folate antagonist that indirectly inhibits cell division by blocking folate-related enzymes required in the pathways of purine and pyrimidine nucleotide synthesis [29]. The controlled and targeted co-delivery of both drugs has been effective against different cancer cell lines, reducing off-target toxicity [30–32].

Here, a light-triggered system for the sequential release of MTX and

* Corresponding author. Physics Centre of Minho and Porto Universities (CF-UM-UP), University of Minho, Campus de Gualtar, 4710-057, Braga, Portugal.
E-mail address: sergiorafael.dasilva@uvigo.gal (S.R.S. Veloso).

https://doi.org/10.1016/j.jddst.2024.105723
Received 4 December 2023; Received in revised form 25 April 2024; Accepted 26 April 2024
Available online 28 April 2024

DOX based on plasmonic chitosan/alginate nanogels was developed. MTX-loaded mesoporous silica-coated gold nanorods were enveloped with a phospholipid bilayer acting as a gatekeeper. The gold nanorods (NRs) enable the conversion of near-infrared (NIR) radiation to heat [33]. The large surface area of the mesoporous silica shell improves drug encapsulation and release, besides enhancing colloidal stability and biocompatibility [34–36]. However, uncapped mesoporous silica is prone to premature drug release, which can lead to undesired side effects to normal cells/tissues during treatment. The capping with a thermoresponsive material, such as a phospholipid bilayer, improves the controlled release by working as a nanovalve that switches on when the heat generated by the NRs increases temperature over the phase transition temperature of the bilayer, thus increasing the release of encapsulated drug. The suitability of this strategy was demonstrated for different therapeutic and diagnostic agents [37,38]. These particles are embedded in a chitosan/alginate nanogel loaded with doxorubicin, which provides an additional barrier to drug diffusion. The nanogels can be easily prepared through a straightforward ionic gelation method using tripolyphosphate (TPP) [39]. Chitosan and alginate are FDA-approved biopolymers with biological properties adequate for biomedical applications, such as low-cost, biocompatibility, biodegradability, and non-toxicity [40,41]. These nanogels have shown promising results in the delivery of a wide variety of therapeutic agents [42–45], and efficient cellular uptake in several cancer cell lines [39]. Besides, the release of the loaded drugs can be enhanced through a thermal stimulus [22].

Hence, this work aimed to develop self-assembled plasmonic nanogels for the delivery and sequential release of DOX and MTX through a NIR light-triggered strategy. The developed nanosystem enables the synergistic effect of hyperthermia and chemotherapy, enhancing antitumor efficacy. The promising results and the simple formulation design point to a great potential for the delivery of other drug combinations in therapeutic applications.

2. Materials and methods

2.1. Materials

Tetrachloroauric acid ($HAuCl_4.3H_2O$), silver nitrate ($AgNO_3$), hydrochloric acid (HCl), L-ascorbic acid (AA), hexadecyltrimethylammonium bromide (CTAB), sodium borohydride ($NaBH_4$), tetraethyl orthosilicate (TEOS), sodium oleate (NaOL), doxorubicin (DOX), methotrexate (MTX), 1,2-dipalmitoyl-*sn*-glycero-3-phosphocholine (DPPC), cholesterol (Ch), sodium alginate (180947, Sigma-Aldrich, 15–25 cP 1 % in H_2O), and chitosan (448869, Sigma-Aldrich, Reykjavik, Iceland, low molecular weight, 75–85 % deacetylation), and tripolyphosphate (TPP) were obtained from Sigma-Aldrich. Ultrapure water Milli-Q® was used in the preparation of all solutions.

2.2. Development of the plasmonic chitosan/alginate nanogels

2.2.1. Preparation of the neat plasmonic nanogels

The gold NRs with an LSPR near 800 nm were prepared through a seedless method described elsewhere [21,46]. Briefly, stock solutions of CTAB and sodium oleate (200 mM) were added for a final concentration of 38 mM and 12.5 mM (final volume 10 mL), respectively, and topped up to 5 mL with Milli-Q water. Then, 5 mL $HAuCl_4$ (1 mM), 240 μL $AgNO_3$ (4 mM), 50 μL HCl (11.7 M), and 75 μL ascorbic acid (85.8 mM) were sequentially added with an interval of 5 min after each addition. Then, 7.5 μL freshly prepared $NaBH_4$ (10 mM) was rapidly injected into the mixture. The stirring was stopped and the mixture was kept at 30 °C for 4 h. The AuNRs were washed twice with Milli-Q and repeating centrifugation at 9000*g* for 30 min. The isolated AuNRs were posteriorly used for addition of mesoporous silica shell, as described elsewhere [21]. The AuNRs were resuspended in CTAB (100 mM), at a final gold concentration of 5 mM. Then, 3.4 mL of a 6 mM CTAB, 10 mL of ethanol and 22.3 mL of water were kept at 30 °C in a 50 mL round beaker under magnetic stirring. After 10 min, 67 μL of NH_4OH (25 vol %) were added, followed by 1 mL of the prepared AuNR solution. After 5 min, 27 μL of TEOS was added dropwise under vigorous stirring, and the reaction mixture was kept at 60 °C for 2 days. The synthesized particles were centrifuged (30 min; 9000 g), and washed in ethanol. To remove the CTAB from the pores, the particles were resuspended in 10 mL ethanol and HCl (1 v/v%) and left under stirring and reflux for 6 h at 60 °C. The particles were washed three times in ethanol by centrifugation (15 min; 9000 g), and redispersed in 1 mL ethanol for further use. The enveloping of the obtained NR@Si mesoporous particles with a phospholipid membrane was adapted from Ref. [37]. Different lipid concentrations for a DPPC:cholesterol 7:3 ratio were tested to optimize the nanoparticles' coverage. A 10 mM lipid solution in chloroform was evaporated with a stream of ultrapure nitrogen gas. Then, 200 μL of an ethanolic dispersion of NRs@Si (0.5 mg/mL) were added to the lipid film, sonicated for 10 min, and evaporated with a stream of ultrapure nitrogen gas. The resulting lipid film was resuspended in 1 mL of ultrapure water. The preparation of plasmonic nanogels was adapted from a method described elsewhere [22,39]. The aqueous dispersion of lipid-gated mesoporous particles was centrifuged (20 min, 9000*g*), the pellet was redispersed in 100 μL of 0.1 wt% TPP, and added drop-by-drop to 900 μL of 0.1 wt% chitosan under vigorous stirring. After 10 min, the solution was diluted 1:1 with ultrapure water, and added drop-by-drop to 2 mL of 0.1 wt% alginate solution under stirring. The pH was adjusted between 7.1 and 7.5 by adding 0.025 mM NaOH. Afterward, the nanogels were centrifuged at 3500*g* for 10 min, and redispersed in 1 mL of 10 mM phosphate buffer pH = 7.4. The dispersion was stored at 4 °C.

2.2.2. Preparation of drug-loaded plasmonic nanogels

Encapsulation of methotrexate in the mesoporous particles was carried out through incubation in acetone for 24 h. Different particle: MTX mass ratios (1:1; 2:1; 3:1; 4:1) were assessed, and the particle mass was fixed at 0.5 mg/mL. The solution was then added over the lipid film, evaporated with ultrapure nitrogen gas stream, redispersed in ethanol, followed by the as-mentioned lipid-gated mesoporous particles preparation. The aqueous solution of lipid-gated mesoporous particles was centrifuged (20 min, 9000 *g*) and the supernatant stored for determination of encapsulated MTX. Loading of the nanogels with DOX was carried out by preparing a 2 mL of sodium alginate 0.1 wt% solution containing 0.1 mg of DOX. As mentioned, the chitosan nanogels were then added drop-by-drop to the former solution to obtained chitosan/alginate nanogels loaded with DOX. The nanogels were centrifuged at 3500*g* for 10 min, redispersed in 1 mL of 10 mM phosphate buffer pH = 7.4, and the supernatant was stored to determine the encapsulated DOX. For the purpose of drug release assays, the nanogels were loaded only with MTX or DOX.

2.2.3. Determination of encapsulated drug and release assays

Encapsulation efficiency of MTX and DOX was determined through UV–vis absorption spectroscopy by measurement of the non-encapsulated content in the mentioned supernatants. The encapsulation efficiency was determined as follows:

$$\mathbf{EE}\ (\%) = \frac{\mathrm{drug}_{\mathrm{total}} - \mathrm{drug}_{\mathbf{non-encapsulated}}}{\mathrm{drug}_{\mathrm{total}}} \times \mathbf{100\%}$$

Nanogels loaded with only methotrexate or doxorubicin were used for the release assays. In microcentrifuge tubes, 100 μL of drug-loaded nanogels (~6 mg/mL) were added. Then, 700 μL of 10 mM phosphate buffer pH = 7.4 or pH = 6 were added to keep pH constant (bottom reservoir); an Amicon® Ultra-0.5 mL centrifugal filter with 0.1 μm pore size was immersed in the bottom reservoir, and filled with 200 μL of buffer (top reservoir), resulting in a dissolution medium with a total volume of 1 mL. The total drug concentration to be released was

determined to be < 100 μM. The system was kept under stirring in an orbital shaker and incubated at room temperature. Aliquots (200 μL) were taken from the top reservoir, and replaced with fresh buffer to maintain sink conditions, and fluorescence (λ_{exc} = 480 nm for DOX [47]; λ_{exc} = 370 nm for MTX [48]) was measured to determine the concentration at each time point. Release assays of free DOX and MTX were carried out (Fig. S1). Fluorescence emission calibration curves of MTX and DOX in pH 6 and pH 7.4 are provided in Supplementary Material (Fig. S1). Limit-of-detection (LOD) and limit-of-quantification (LOQ) were calculated from the calibration curves as $\frac{3.3\sigma}{S}$ and $\frac{10\sigma}{S}$, respectively, in which σ is the standard deviation of y-intercept and S is the slope of the calibration curve (Table S1). For the assays with laser irradiation at 808 nm (1 W/cm^2), the samples were irradiated for 10 min after each aliquot. Release profile assays were performed in triplicate.

2.3. Characterization techniques

2.3.1. General spectroscopic methods

Absorption spectra were recorded using a Shimadzu UV-3600 Plus UV–Vis–NIR spectrophotometer (Shimadzu Corporation, Kyoto, Japan). Fluorescence measurements were carried out using a Horiba-Jobin Yvon Fluorolog 3 spectrofluorimeter. FTIR spectra were measured using a PerkinElmer Spectrum Two™ IR spectrometer (PerkinElmer Inc., Waltham, MA, USA) with an attenuated total reflectance (ATR) accessory. The average hydrodynamic diameter and zeta potential of the nanoparticles (n = 3 independent runs) were measured in 10 mM phosphate buffer pH 7.4 at 0.01 mg/mL in a Dynamic Light Scattering (DLS) equipment Litesizer™ 500 from Anton Paar (Anton Paar GmbH, Graz, Austria), using a semiconductor laser diode of 40 mW and λ = 658 nm, a backscatter angle (175°), and a controlled temperature of 25 °C.

2.3.2. Photothermia measurements

To obtain the photothermia profiles upon irradiation of the nanoparticles, the sample (200 μL) was prepared in a 0.4 cm polystyrene cuvette, placed in a sample cuvette holder with the temperature stabilized at 25 °C, and irradiated with an 808 nm laser. The temperature was measured by placing a K-type thermocouple 1 cm inside the sample. The samples were irradiated at 1 W/cm^2 at different concentrations and with deionized water as a negative control until the suspension reached a steady-state temperature to calculate the photothermal conversion efficiency. The photothermal stability of nanoparticles was studied by irradiating the samples for 3 min, followed by cooling to room temperature without laser irradiation for 6 cycles. The photothermal conversion efficiency was calculated from the equation [49,50]:

$$\eta = \frac{hS(T_{max} - T_{surr}) - Q_{dis}}{I\left(1 - 10^{-A_{808}}\right)}$$

where T_{max} is the equilibrium temperature, T_{surr} is the surrounding temperature, h is the heat transfer coefficient, S is the surface area of the container, Q_{dis} is the heat dissipation from the light absorbed by the solvent and container, I is the laser power, and A_{808} is the samples absorbance at 808 nm. The time constant (τ_s) was obtained through the linear fitting of the equation to the cooling phase:

$$t = -\tau_s \, ln \frac{T - T_{surr}}{T_{max} - T_{surr}}$$

The obtained value of τ_s enabled the calculation of $hS = \mathbf{mC}/\tau_s$, in which m = 0.2 g and **C** = 4.185 J/g/K are the mass and specific heat

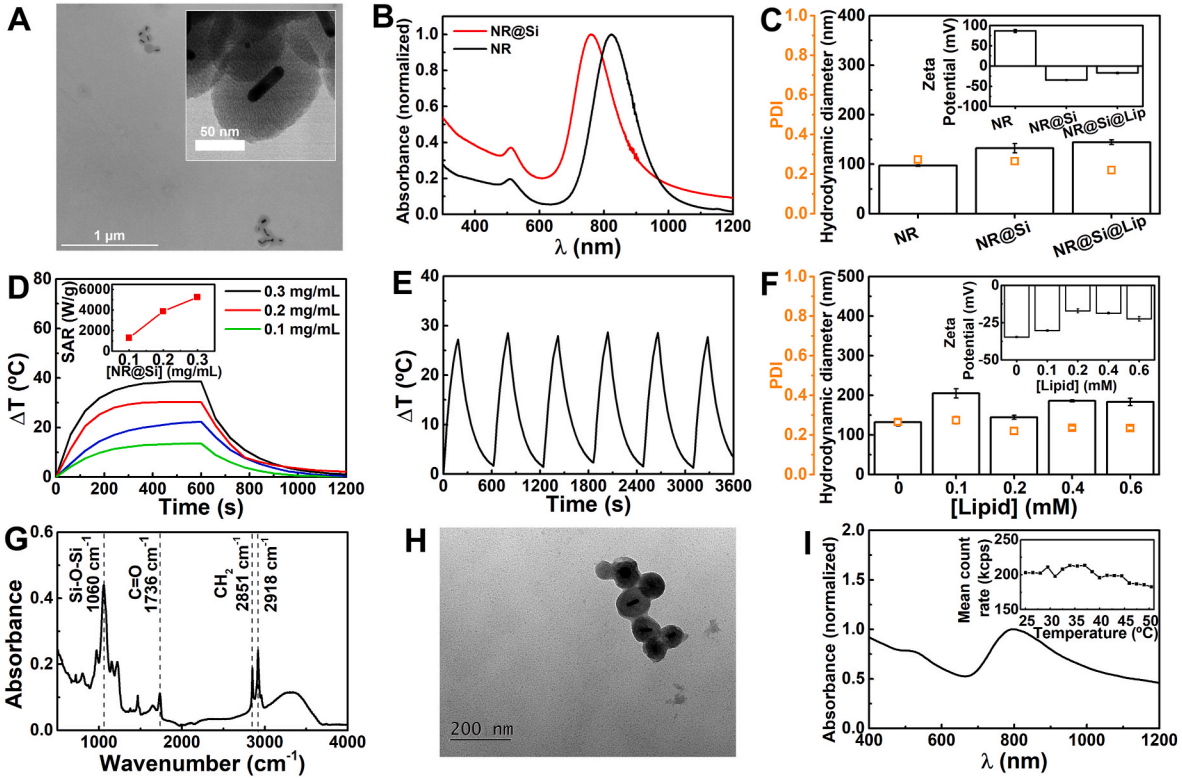

Fig. 1. (A) STEM image of mesoporous silica-coated gold nanorods (NR@Si). Inset: HR-TEM image of NR@Si. (B) UV–vis absorption spectra of gold nanorods (NR), and NR@Si. (C) Hydrodynamic diameter and polydispersity (PDI) of NR, NR@Si, and lipid-gated mesoporous silica-coated gold nanorods (NR@Si@Lip). Inset: Zeta potential of the respective particles. (D) Heating profiles of different concentrations of NR@Si under 808 nm laser irradiation (1 W/cm^2). Inset: Specific absorption rate (SAR) dependence on the particle concentration. (E) Heating cycles of NR@Si nanoparticles at 0.3 mg/mL under 808 nm laser irradiation (1 W/cm^2). (F) Hydrodynamic size, and polydispersity of NR@Si@Lip prepared with variable lipid concentration. The NR@Si nanoparticles were kept at a fixed concentration of 0.1 mg/mL. Inset: Zeta potential of the respective particles. (G) FTIR spectrum of the NR@Si@Lip. (H) TEM image of NR@Si@Lip nanoparticles. (I) Normalized UV/vis/NIR absorption spectrum of NR@Si@Lip. Inset: Dependence on temperature of the mean count rate of NR@Si@Lip.

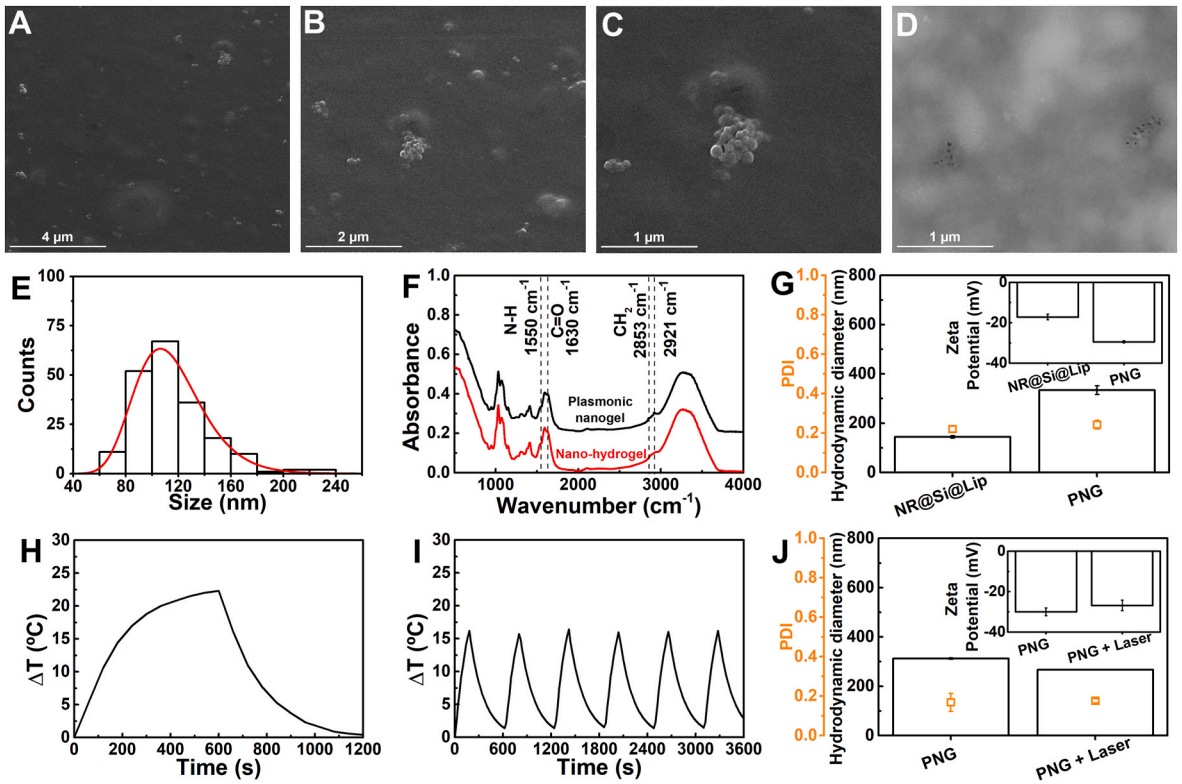

Fig. 2. (A–C) SEM images of plasmonic nanogels with different magnifications. (D) STEM image and (E) size histogram of plasmonic nanogels. (F) FTIR spectra of nano-hydrogel (red) and plasmonic nanogel (black). (G) Comparison of the hydrodynamic diameter, polydispersity and zeta potential of plasmonic nanogels (PNG) with the lipid-gated mesoporous silica-coated gold nanorods (NR@Si@Lip). (H) Heating profile of plasmonic nanogels under 808 nm laser irradiation (1 W/cm^2) at 2 mg/mL, and the respective (I) heating cycles. (J) Comparison of the hydrodynamic diameter, polydispersity and zeta potential of plasmonic nanogels (PNG) with and without exposure to six cycles of 808 nm laser irradiation (1 W/cm^2).

capacity of water in the cuvette, respectively.

2.4. Biological assays

2.4.1. Cell culture

HEK293 cells, derived from primary embryonic human kidney, and human SH-SY5Y neuroblastoma cells were grown at 37 °C, in a humid 5 % CO_2, in Dulbecco's Modified Eagle's medium (Gibco) supplemented with 10 % heat-inactivated fetal bovine serum (Gibco), 1 % antibiotics (penicillin 100 U/mL and streptomycin 100 μg/mL) (Gibco), and 1 % L-glutamine (Gibco). U373 MG human glioma cell cultures were kept at 37 °C and 5 % CO_2 under sterile conditions in Dulbecco's modified Eagle's medium (Gibco), supplemented with 10 % fetal bovine serum (Gibco, plus 1 % antibiotics (penicillin 100 U/mL and streptomycin 100 μg/mL) (Gibco).

2.4.2. Cell viability

The effect of plasmonic nanogels with and without drugs on the survival of U373 human glioma cells, SH-SY5Y human neuroblastoma and HEK293 cell lines was determined by the MTT assay (3-[4,5-dimethylthiazol-2-yl]- 2,5-diphenyltetrazolium bromide), using the Cell Proliferation Kit I (Roche Diagnostics, Mannheim, Germany). The cells were expanded, cultured in a 96-well plate, and treated with various concentrations of nanogels. Methanol 10 % and Triton X-100 % culture media were used as the positive and negative controls, respectively. MTT solution was added to each well 24 h after treatment, and the plates were then incubated for 3 h at 37 °C. MTT, which is soluble in water, is transformed into insoluble formazan by succinate dehydrogenase within the mitochondria via tetrazolium ring cleavage. After the supernatant was removed, 100 μL DMSO (Sigma) was added and the optical density was estimated at 590 nm using an ELISA reader as described in the MTT assay protocol.

2.5. Statistics

Characterization and drug release assays were performed in triplicate (n = 3), and the results were displayed as mean ± standard deviation. Regarding the biological assays, the assays were performed with n = 6, and the GraphPad Prism 7 software (GraphPad Software Inc., San Diego, CA, EUA) was used to manage the resulting data and to perform the statistical analysis. A two-sample Student's t-test was used to analyse differences between different groups. Statistically significant results are assumed considering a p-value ≤0.05. Analysis of Variance (ANOVA) is a statistical tool used to determine each factor's importance in an outcome. Tukey's multiple comparisons were used to evaluate and compare compressive and flexural strength values using a one-way ANOVA test at a p-value of 0.05.

3. Results and discussion

3.1. Characterization of the lipid-gated mesoporous silica-coated gold nanorods

Replicas of the synthesized gold nanorods display LSPR and TSPR bands maxima of 814 ± 9 nm and 509 nm (corresponding to an aspect ratio >3.5) [46], respectively, and an average LSPR-to-TSPR ratio of 5.05 ± 0.06 (Fig. S2), which is indicative of good shape purity [51,52]. The addition of the mesoporous silica shell afforded nanoparticles with an average particle size of 99 ± 11 nm, and a blueshift of the LSPR band to ~760 nm, as described elsewhere (Fig. 1A, B and S2 in Supplementary Material) [21]. This blue-shift can be associated with the smaller overall refractive index of the mesoporous silica coating around gold nanorods

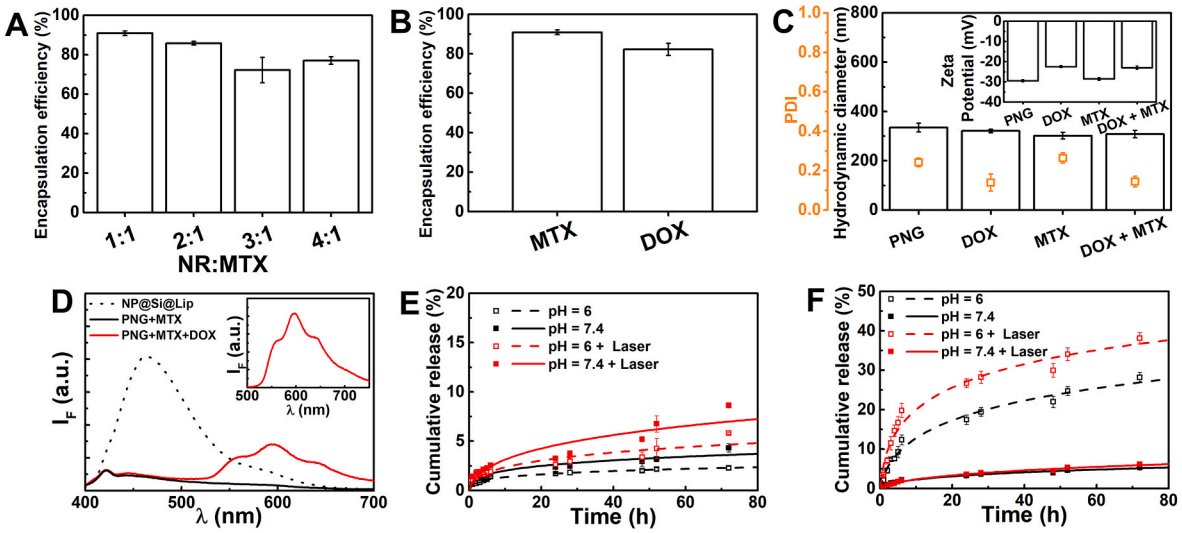

Fig. 3. (A) Encapsulation efficiency of methotrexate (MTX) obtained for several NR:MTX ratios. (B) Comparison of the encapsulation efficiency of methotrexate (MTX) and doxorubicin (DOX) in plasmonic lipogels (1:1 drug:NR ratio). (C) Comparison of the hydrodynamic diameter, polydispersity and zeta potential of neat plasmonic nanogels (PNG) and loaded with MTX and/or DOX. (D) Fluorescence emission of MTX (λ_{exc} = 370 nm) in lipid-gated mesoporous silica-coated gold nanorods (NR@Si@Lip), plasmonic nanogels loaded with MTX (PNG + MTX) and DOX (PNG + DOX + MTX). Inset: Fluorescence emission of doxorubicin (λ_{exc} = 480 nm) in plasmonic nanogels loaded with MTX and DOX. Cumulative release of (E) MTX and (F) DOX from plasmonic nanogels in pH = 6 and pH = 7.4 with and without exposure to laser irradiation (808 nm, 1 W/cm^2, 10 min after each aliquot). The release profiles were fitted to Gompertz model over 76 h.

surface than the CTAB coating, as described by Wu et al. [53]. TEM images and EDS mapping (Fig. 1A–S3 and S4) indicated the presence of silica particles containing a single nanorod, and also without nanorods.

DLS measurements were also carried out, in which the hydrodynamic size corresponds to a spherical particle with a diffusion coefficient equivalent with the measured particles [54]. The intensity distribution profiles of gold nanorods displayed contributions under 10 nm that can be associated with the presence of CTAB micelles (Fig. S5). These particles also exhibit a positive zeta potential (87 ± 3 mV) and a hydrodynamic size of 97 ± 1 nm (Fig. 1C and Table S2). A larger hydrodynamic size (132 ± 9 nm) and a single intensity distribution peak were obtained after addition of the mesoporous silica shell. Yet, the broadness indicated some polydispersity (PDI ~0.27), which is in agreement with the TEM results. The negative zeta potential (−35 mV) also confirmed the coating with silica, and suggested the good stability of the nanoparticles. The latter is further supported by the lack of noise in the correlograms (absence of sedimentation).

The mesoporous silica-coated gold nanorods exhibited great heating generation upon laser irradiation at 808 nm (1 W/cm^2), as well as good photostability over several irradiation cycles, as displayed in Fig. 1D and E. The incremental particle content led to a larger heating generation, reaching a ΔT ~40 °C in 10 min at 0.3 mg/mL. A high heating efficiency of 83 ± 2 % was obtained, which is in the range of the commonly reported values for mesoporous silica-coated gold nanorods [55,56]. Additionally, as described in other works [57], SAR values slightly increased with concentration, suggesting that under these conditions light absorption is homogeneous along the nanoparticles' suspension.

Different lipid concentrations, for a DPPC:cholesterol 7:3 ratio, were initially assessed (Fig. 1F). A lipid concentration of 0.2 mM for 0.1 mg/mL of mesoporous nanoparticles afforded a smaller size (144 ± 5 nm), lower PDI (~0.22) and less negative zeta potential (−17 ± 1 mV) among the tested formulations (0.1–0.6 mM lipid concentration), indicating a suitable coverage of the particles. Fig. 1C provides a comparison of the lipid-gated nanoparticles (NR@Si@Lip) with the neat nanorods (NRs) and silica-coated nanoroads (NR@Si). The coating with a phospholipid bilayer was also evaluated by FTIR spectroscopy (Fig. 1G). The peak near 1060 cm^{-1} is assigned to the mesoporous silica shell Si–O–Si vibration. The peaks near 2851 cm^{-1} and 2918 cm^{-1} can be assigned to symmetric and anti-symmetric CH_2 stretching, and the C═O deformation is assigned to the peak near 1736 cm^{-1}, thus confirming the attachment of the lipid bilayer to the surface of mesoporous particles [37]. TEM images further supported the adsorption of the lipid bilayer (Fig. 1H). The LSPR band remained unaffected by the addition of the lipid bilayer (Fig. 1I), as described elsewhere [37]. Regarding the stability, the NR@Si@Lip particles displayed a slight increase (~10 nm) of the hydrodynamic diameter with increasing temperature, from 25 °C to 50 °C (Fig. S6), and the temperature dependence of the mean count rate also suggested the phase transition of the lipid bilayer near 40 °C (Fig. 1H inset). Nevertheless, the low polydispersity (~0.2) remained mostly unchanged across the evaluated temperature range, thus indicating the good stability of the nanoparticles.

3.2. Characterization of the plasmonic nanogels

Electron microscopy images of nanogels containing the lipid-gated mesoporous silica-coated gold nanorods (Fig. 2A–D), hereafter referred as plasmonic nanogels (PNG), revealed the presence of rounded particles and some agglomerates, which can result from the drying process of the samples and/or the nanogels containing cluster of nanoparticles. Additional SEM and TEM images are included in Fig. S7 that further suggest nanogels comprising a single or a cluster of nanoparticles. Similar observations were described for chitosan/alginate nanogels containing magnetic multicore nanoparticles [22]. The nanogels displayed an average size of 115 ± 28 nm (Fig. 2E), which indicates that the nanogels are mostly comprised of a single NR@Si@Lip particle (99 ± 11 nm). It is worth pointing out that electron microscopy is performed under vacuum and thus, the obtained size corresponds to a collapsed state of the nanogel. Besides, the images further suggest the nanogels to be non-porous, providing a slow drug release rate [58,59], which is useful for controlled and sustained release of the encapsulated drugs in stimuli-responsive systems.

FTIR spectra of nano-hydrogels (without encapsulated nanoparticles) and plasmonic nanogels are displayed in Fig. 2F. Characteristic wavenumbers for chitosan and alginate are highlighted [60–63]. The main peaks were detected near 1630 cm^{-1} (C═O stretching), and 1550 cm^{-1} (N–H bending vibrations). Other peaks include 1414 cm^{-1} (C═O), 1157 cm^{-1} (asymmetric stretching of the C–O–C bridge of the saccharide rings), 1077 cm^{-1} and 1035 cm^{-1} (commonly assigned to the

stretching of the C–O–C bond of the glycosidic links in chitosan and alginate, respectively). The peaks of lipid bilayer near 2853 cm^{-1} and 2921 cm^{-1} were also identified in the plasmonic nanogels. The dominating contributions of chitosan/alginate nanogel matrix indicates that the NR@Si@Lip particles were successfully encapsulated in the nanogel matrix. Besides, comparison of nano-hydrogels and plasmonic nanogels shows that no significant differences were obtained in the peaks' wavenumbers due to the interactions between the nanogel matrix and the composites.

The resulting plasmonic nanogels displayed good polydispersity, strongly negative zeta potential in 10 mM phosphate buffer pH = 7.4 (near −30 mV), and a hydrodynamic size larger than 300 nm. The larger size from DLS is associated with the swellable ability of chitosan/alginate polymers [22,39,60,64]. The negative charge is a result of alginate consisting of alternating blocks of β-(1 → 4)-linked-D-mannuronic acid and α-(1 → 4)-linked-L-glucuronic acid [65], and closely matches other reported values [60,66]. Besides, it indicates that the nanogels display good colloidal stability, and that aggregation might be averted (also suggested by the correlogram in Fig. S8).

The plasmonic nanogels exhibited great heat generation (Fig. 2H) and photostability (Fig. 2I) upon several cycles of laser irradiation (808 nm, 1 W/cm^2). The light-to-heat conversion efficiency decreased to a value of 30 ± 1 % compared to the mesoporous silica-coated gold nanorods, possibly due to the additional scattering by the nanogel matrix. Besides, after irradiation, the hydrodynamic size was found to slightly decrease (Fig. 2J), and the zeta potential became less negative, possibly due to some heat-induced depolymerization of the nanogel's alginate shell, and consequent exposure of positively-charged chitosan matrix. The presence of smaller particles after irradiation was suggested by the intensity distributions (Fig. S9 in Supplementary Material).

3.3. Drug loading of plasmonic nanogels

Initially, several NR:MTX ratios were assessed to optimize MTX loading (Fig. 3A–S10). The best encapsulation efficiency (EE% ~ 90 %) was obtained for 1:1 ratio, which afforded MTX-loaded NR@Si@Lip particles with an average hydrodynamic size of 153 ± 8 nm, low PDI (0.21 ± 0.02), and similar zeta potential (−20 ± 1 mV) to the unloaded nanoparticles. Following these results, the NR:DOX ratio was also kept at 1:1 (Fig. 3B), displaying an encapsulation efficiency near 85 %, which is similar to other reported values [22].

The loading of nanogels with DOX and MTX did not induce major changes in the hydrodynamic diameter and polydispersity (Fig. 3C and Fig. S11). The latter remained close/within the 0.1–0.2 range, which is considered acceptable for drug delivery applications [67]. A slight decrease of the zeta potential was obtained upon encapsulation of DOX. This is a result of the positive charge of DOX, leading to a screening of the negatively charged groups of alginate through electrostatic interactions [68]. Nonetheless, the negative zeta potential suggests an absence of free DOX amino groups on the nanoparticles surface, which aligns with the high encapsulation efficiency. Besides, the mean diameter around 300 nm was reported to be suitable for intravenous injection of chitosan/alginate nanogels [68].

The fluorescence of MTX and DOX further confirmed the loading in the plasmonic nanogels (Fig. 3D). In the case of MTX, the incorporation of MTX-loaded NR@Si@Lip nanoparticles in the nanogels led to a quenching of MTX fluorescence emission, possibly due to a stronger light scattering by the nanogel matrix. In the presence of DOX, no Förster Resonance Energy Transfer (FRET) is observed between both drugs, which is indicative that the distance between them is larger than 10 nm. This is in line with a nanogel architecture in which MTX is compartmentalized in the mesopores of the NR@Si@Lip nanoparticles, and separated by a thick layer from the location of DOX (electrostatically interacts with the outer layer of alginate) that comprises the chitosan matrix and the lipid bilayer. The strong fluorescence emission of doxorubicin, with maximum near 595 nm, further suggests its location near a weakly polar environment, as described elsewhere [22]. Yoncheva et al. [68] demonstrated that DOX could establish electrostatic, dipole-dipole and hydrophobic interactions with alginate through molecular interactions. Besides, chitosan/alginate nanogels were reported to improve drug stability, cytotoxicity against cancer cells and reduce the cardiotoxic effects of DOX [45].

3.4. Drug release assays of plasmonic nanogels

The release of MTX and DOX was carried out at pH = 6 and pH = 7.4, to assess the pH effect and to simulate the acidic pH conditions of tumour microenvironment and the slightly alkaline pH of physiological media [69,70], respectively. The release profiles of both drugs were biphasic as displayed in Fig. 3E and F, exhibiting an initial phase of faster release followed by a sustained release during the longer second phase. In the case of DOX, the burst effect was more pronounced in the lower pH medium, in which near 25 % was released after 3 days vs. the 5 % in the neutral medium. This is in line with the higher hydrophilicity of DOX at an acidic pH, facilitating its release, as well as the strong interaction between DOX and alginate at neutral pH, due to the ionization of the amino-groups of DOX and the carboxylic groups of alginate chains. The strong interaction between DOX and alginate is also inferred by the drug not being completely released after 3 days. The slow release at neutral pH is advantageous, as it can reduce the drug loss until the system reaches the slightly acidic tumour tissue. Similar results were reported for other drug delivery systems [68,71–74]. Besides, the release profiles indicate that the developed plasmonic nanogels display improved pH-responsiveness and sustained release of DOX than other chitosan and/or alginate nanogels [68,75,76]. Regarding the release profiles of MTX, the sustained release and shallow burst effect is indicative of the strong diffusion barriers caused by the lipid bilayer and gel matrix. Below the phase transition temperature, the lipid bilayer is in the gel phase, which offers increased resistance to the diffusion of MTX out of the mesopores. The chitosan matrix is positively charged at acidic pH, which can electrostatically interact with the negative carboxylate groups of MTX (pK_a near 4.8 and 5.5) [77], thus hindering its release. However, this effect is expected to diminish at neutral pH due to deprotonation of the chitosan primary amines (pK_a ~6.5) [78]. Additionally, MTX has enhanced solubility at neutral pH compared to the acidic pH [79,80]. Yet, the difference between both pH conditions is small, indicating that the system displays improved sustained release when compared to other systems for delivery of MTX [81–85].

The drug release was also assessed under laser irradiation, considering the need of a trigger that enhances drug release, improving the control of the system to minimize size effects of DOX and MTX, and increasing the efficacy of the therapeutic strategy. In general, the results showed that irradiation with an 808 nm laser (1 W/cm^2) led to a slight enhancement of the release in the initial 24 h, and also after each irradiation period during the slower phase. In the case of DOX, the active release was strongly pronounced at pH = 6, while, at pH = 7.4, the heating by the gold nanorods was not enough to enhance its release, thus being comparable to the passive release. This effect is clinically advantageous, as drug release can be spatially enhanced and controlled within tumors and their proximity. Regarding MTX, the photothermia effect produced similar changes in total drug release for both pH conditions. In this sense, the developed plasmonic nanogel enables the sequential release of DOX and MTX, in which the underlaying mechanism can be understood as follows: 1) DOX and MTX are compartmentalized in different components of the nanogel; 2) DOX release is hampered by the nanogel matrix, while MTX release is also hindered by the lipid bilayer covering the mesoporous particles; 3) DOX is initially released at a faster rate in acidic pH owing to the greater hydrophilicity, and weaker electrostatic interactions between DOX and alginate in acidic conditions; 4) photothermia effect enhances the release of MTX by inducing both the lipid bilayer phase transition and thermally increasing the diffusion. Hence, having in mind the need to maintain drugs at target sites with

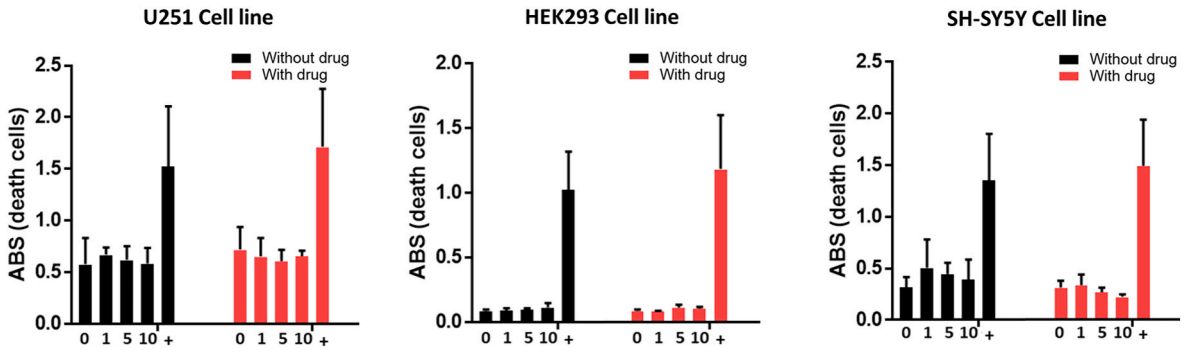

Fig. 4. In vitro cell cytotoxicity assays of plasmonic nanogel in three different cell lines (left graph U251 cell line, middle graph HEK293 cell line and right graph SH-SY5Y cell line). Different doses of plasmonic nanogel (0, 1, 5 and 10 μg/mL) at 24 h, with and without drugs. Data is represented as mean ± SD, and n = 6. There was no cytotoxic effect with any cell line at any of the doses used.

therapeutic concentrations, as well as to tune the release rate and duration, the developed plasmonic nanogels hold promise for the sequential delivery of doxorubicin and methotrexate.

Mathematical models were fitted to the drug release profiles (Table S3), including the Korsmeyer-Peppas and Gompertz models [86]. The fitting analysis of DOX and MTX release profiles revealed that the results could be better described by the Korsmeyer-Peppas model, which can be applied to different system geometries in perfect sink conditions [86,87]. The Gompertz empirical model was also employed for comparison of the release kinetics, also providing a good fitting of the release profiles.

The parameter n of the Korsmeyer-Peppas model is an indicator of the diffusion mechanism (Table S4). In the case of MTX, n values < 0.5 were obtained during the initial 6 h of the release profile, which are indicative of a diffusion-controlled release mechanism, while DOX release displayed n values > 0.85, associated with the swelling or relaxation of network chains. The DOX release mechanism could be associated with its location in the nanogel outer layer, as a result of the preparation method. Besides, the release mechanism remained unchanged despite the photothermia effect, mainly displaying an increase of the release rate constant. Hence, the results suggest the stability of the system under irradiation, as the release mechanism remains unchanged, while the drug release rate is enhanced.

In line with other chitosan/alginate nanogels [42–45], cytotoxicity assays in different cell lines (Fig. 4) revealed that both the neat and drug-loaded plasmonic nanogels are cytocompatible, thus suggesting that undesired side effects can be averted. The co-delivery of MTX and DOX has been described to synergistically inhibit the growth of cancer cells [31,32,85,88]. Li et al. [32] reported self-assembled pH-responsive nanomicelles, in which DOX and MTX synergistically enhanced the antitumor efficacy against different cell lines, including breast cancer cell lines. Rajeev et al. [85] developed a graphene oxide-containing anionic nanocarrier, which displayed pH-responsiveness and synergistic effect against breast cancer in *in vitro* assays. However, among these works, the release profiles commonly display a burst release of the loaded drug, surpassing 20 % in the first 10 h. Considering the heterogeneity of tumour microenvironment, this burst can result in the premature release of the content and lead to undesired side effects to healthy cells/tissues. Hence, in this work, the sustained and sequential release, pH-responsiveness and photothermia capability can provide a suitable strategy to improve the control of drug release, avert undesired side effects and synergistically enhance the therapeutic efficacy.

4. Conclusions

In this work, lipid-gated mesoporous silica-coated gold nanorods with an average hydrodynamic diameter of 144 ± 5 nm were developed. The particles exhibited an LSPR near 800 nm, negative zeta potential (~−17 mV), and could be formulated into chitosan/alginate plasmonic nanogels through a self-assembly method. The obtained plasmonic nanogels with hydrodynamic diameters near 300 nm, low polydispersity (~0.2), and negative zeta potential (~−30 mV), displayed high doxorubicin (EE% ~ 85 %) and methotrexate (EE% ~ 90 %) loading efficiency. Besides, physicochemical characterization suggested the good stability of the nanosystem, but long-term stability studies are yet to be conducted. Both doxorubicin and methotrexate were released with a sustained profile, in which the release of the former was dominated by the swelling or relaxation of network chains, while the latter's release was driven by a diffusion-controlled mechanism. Additionally, the drug release was sequential, in which doxorubicin was released at a faster rate than methotrexate under acidic conditions. In neutral conditions, both drugs were released at a slow rate. Besides, the release could be enhanced through the photothermia effect achieved under NIR (808 nm) laser irradiation. Overall, the chitosan/alginate plasmonic nanogels displayed promising results for controlled and sequential drug release, with potential application in cancer therapy.

CRediT authorship contribution statement

Filipa Costa-e-Sá: Writing – original draft, Visualization, Investigation, Formal analysis. **María Comís-Tuche:** Investigation, Formal analysis. **Carlos Spuch:** Investigation, Formal analysis. **Elisabete M.S. Castanheira:** Writing – review & editing, Validation, Supervision, Conceptualization. **Sérgio R.S. Veloso:** Writing – review & editing, Writing – original draft, Methodology, Investigation, Formal analysis, Conceptualization.

Declaration of competing interest

The authors declare the following financial interests/personal relationships which may be considered as potential competing interests: Sergio R.S. Veloso reports financial support was provided by Foundation for Science and Technology. If there are other authors, they declare that they have no known competing financial interests or personal relationships that could have appeared to influence the work reported in this paper.

Data availability

Data will be made available on request.

Acknowledgements

This work was funded by the Portuguese Foundation for Science and Technology (FCT) in the framework of the Strategic Funding of CF-UM-UP (UIDB/04650/2020, UIDP/04650/2020) and University of Minho

through the "Prémio UMinho de Iniciação na Investigação Científica 2023". C.S. was funded by Instituto de Salud Carlos III/FEDER grant number PI20/00937, and "Axencia Galega de Innovación" grant number IN607B-2018/17. S.R.S. Veloso acknowledges FCT for a PhD grant (SFRH/BD/144017/2019 and COVID/BD/153440/2023). Support from MAP-Fis Doctoral Programme is also acknowledged.

Appendix ASupplementary data

Supplementary data to this article can be found online at https://doi.org/10.1016/j.jddst.2024.105723.

References

[1] P. Zhang, A. Fischer, Y. Ouyang, J. Wang, Y.S. Sohn, R. Nechushtai, E. Pikarsky, C. Fan, I. Willner, Aptamer-modified DNA tetrahedra-gated metal–organic framework nanoparticle carriers for enhanced chemotherapy or photodynamic therapy, Chem. Sci. 12 (2021) 14473–14483, https://doi.org/10.1039/D1SC04229G.

[2] R. De Souza, P. Zahedi, C.J. Allen, M. Piquette-Miller, Polymeric drug delivery systems for localized cancer chemotherapy, Drug Deliv. 17 (2010) 365–375, https://doi.org/10.3109/10717541003762854.

[3] R.B. Mokhtari, T.S. Homayouni, N. Baluch, E. Morgatskaya, S. Kumar, B. Das, H. Yeger, Combination therapy in combating cancer, Oncotarget 8 (2017) 38022–38043, https://doi.org/10.18632/oncotarget.16723.

[4] B.G. Carvalho, F.F. Vit, H.F. Carvalho, S.W. Han, L.G. de la Torre, Recent advances in co-delivery nanosystems for synergistic action in cancer treatment, J. Mater. Chem. B 9 (2021) 1208–1237, https://doi.org/10.1039/D0TB02168G.

[5] S. Fumoto, K. Nishida, Co-Delivery systems of multiple drugs using nanotechnology for future cancer therapy, Chem. Pharm. Bull. 68 (2020) 603–612, https://doi.org/10.1248/cpb.c20-00008.

[6] S. Lou, Z. Zhao, M. Dezort, T. Lohneis, C. Zhang, Multifunctional nanosystem for targeted and controlled delivery of multiple chemotherapeutic agents for the treatment of drug-resistant breast cancer, ACS Omega 3 (2018) 9210–9219, https://doi.org/10.1021/acsomega.8b00949.

[7] A.C. Krauss, X. Gao, L. Li, M.L. Manning, P. Patel, W. Fu, K.G. Janoria, G. Gieser, D. A. Bateman, D. Przepiorka, Y.L. Shen, S.S. Shord, C.M. Sheth, A. Banerjee, J. Liu, K. B. Goldberg, A.T. Farrell, G.M. Blumenthal, R. Pazdur, FDA approval summary: (daunorubicin and cytarabine) liposome for injection for the treatment of adults with high-risk acute myeloid leukemia, Clin. Cancer Res. 25 (2019) 2685–2690, https://doi.org/10.1158/1078-0432.CCR-18-2990.

[8] T. Jiang, R. Mo, A. Bellotti, J. Zhou, Z. Gu, Gel–liposome-Mediated Co-delivery of anticancer membrane-associated proteins and small-molecule drugs for enhanced therapeutic efficacy, Adv. Funct. Mater. 24 (2014) 2295–2304, https://doi.org/10.1002/adfm.201303222.

[9] T. Lang, Y. Liu, Z. Zheng, W. Ran, Y. Zhai, Q. Yin, P. Zhang, Y. Li, Cocktail strategy based on spatio-temporally controlled nano device improves therapy of breast cancer, Adv. Mater. 31 (2019), https://doi.org/10.1002/adma.201806202.

[10] J. Huang, Y. Xu, H. Xiao, Z. Xiao, Y. Guo, D. Cheng, X. Shuai, Core–shell distinct nanodrug showing on-demand sequential drug release to act on multiple cell types for synergistic anticancer therapy, ACS Nano 13 (2019) 7036–7049, https://doi.org/10.1021/acsnano.9b02149.

[11] T. Liu, L. Lai, Z. Song, T. Chen, A sequentially triggered nanosystem for precise drug delivery and simultaneous inhibition of cancer growth, migration, and invasion, Adv. Funct. Mater. 26 (2016) 7775–7790, https://doi.org/10.1002/adfm.201604206.

[12] P. Zhao, S. Wang, J. Jiang, Y. Gao, Y. Wang, Y. Zhao, J. Zhang, M. Zhang, Y. Huang, Targeting lactate metabolism and immune interaction in breast tumor via protease-triggered delivery, J. Contr. Release 358 (2023) 706–717, https://doi.org/10.1016/j.jconrel.2023.05.024.

[13] K. Wang, B. Yang, H. Ye, X. Zhang, H. Song, X. Wang, N. Li, L. Wei, Y. Wang, H. Zhang, Q. Kan, Z. He, D. Wang, J. Sun, Self-strengthened oxidation-responsive bioactivating prodrug nanosystem with sequential and synergistically facilitated drug release for treatment of breast cancer, ACS Appl. Mater. Interfaces 11 (2019) 18914–18922, https://doi.org/10.1021/acsami.9b03056.

[14] S. Ahmadi, N. Rabiee, M. Bagherzadeh, F. Elmi, Y. Fatahi, F. Farjadian, N. Baheiraei, B. Nasseri, M. Rabiee, N.T. Dastjerd, A. Valibeik, M. Karimi, M. R. Hamblin, Stimulus-responsive sequential release systems for drug and gene delivery, Nano Today 34 (2020) 100914, https://doi.org/10.1016/j.nantod.2020.100914.

[15] D. Wan, Y. Yang, Y. Liu, X. Cun, M. Li, S. Xu, W. Zhao, Y. Xiang, Y. Qiu, Q. Yu, X. Tang, Z. Zhang, Q. He, Sequential depletion of myeloid-derived suppressor cells and tumor cells with a dual-pH-sensitive conjugated micelle system for cancer chemoimmunotherapy, J. Contr. Release 317 (2020) 43–56, https://doi.org/10.1016/j.jconrel.2019.11.011.

[16] S. Shen, H.-J. Li, K.-G. Chen, Y.-C. Wang, X.-Z. Yang, Z.-X. Lian, J.-Z. Du, J. Wang, Spatial targeting of tumor-associated macrophages and tumor cells with a pH-sensitive cluster nanocarrier for cancer chemoimmunotherapy, Nano Lett. 17 (2017) 3822–3829, https://doi.org/10.1021/acs.nanolett.7b01193.

[17] S.R.S. Veloso, P.J. Jervis, J.F.G. Silva, L. Hilliou, C. Moura, D.M. Pereira, P.J. G. Coutinho, J.A. Martins, E.M.S. Castanheira, P.M.T. Ferreira, Supramolecular ultra-short carboxybenzyl-protected dehydropeptide-based hydrogels for drug delivery, Mater. Sci. Eng. C 122 (2021) 111869, https://doi.org/10.1016/j.msec.2021.111869.

[18] X. Lai, X. Liu, H. Pan, M. Zhu, M. Long, Y. Yuan, Z. Zhang, X. Dong, Q. Lu, P. Sun, J. F. Lovell, H. Chen, C. Fang, Light-triggered efficient sequential drug delivery of biomimetic nanosystem for multimodal chemo-, antiangiogenic, and anti-MDSC therapy in melanoma, Adv. Mater. 34 (2022), https://doi.org/10.1002/adma.202106682.

[19] L. Wang, Y. Chang, Y. Feng, X. Li, Y. Cheng, H. Jian, X. Ma, R. Zheng, X. Wu, K. Xu, H. Zhang, Nitric oxide stimulated programmable drug release of nanosystem for multidrug resistance cancer therapy, Nano Lett. 19 (2019) 6800–6811, https://doi.org/10.1021/acs.nanolett.9b01869.

[20] L. Zhang, M. Zhang, L. Zhou, Q. Han, X. Chen, S. Li, L. Li, Z. Su, C. Wang, Dual drug delivery and sequential release by amphiphilic Janus nanoparticles for liver cancer theranostics, Biomaterials 181 (2018) 113–125, https://doi.org/10.1016/j.biomaterials.2018.07.060.

[21] S.R.S. Veloso, V. Gomes, S.L.F. Mendes, L. Hilliou, R.B. Pereira, D.M. Pereira, P.J. G. Coutinho, P.M.T. Ferreira, M.A. Correa-Duarte, E.M.S. Castanheira, Plasmonic lipogels: driving co-assembly of composites with peptide-based gels for controlled drug release, Soft Matter 18 (2022) 8384–8397, https://doi.org/10.1039/D2SM00926A.

[22] S.R.S. Veloso, E.S. Marta, P.V. Rodrigues, C. Moura, C.O. Amorim, V.S. Amaral, M. A. Correa-Duarte, E.M.S. Castanheira, Chitosan/alginate nanogels containing multicore magnetic nanoparticles for delivery of doxorubicin, Pharmaceutics 15 (2023) 2194, https://doi.org/10.3390/pharmaceutics15092194.

[23] Z. Han, M. Gao, Z. Wang, L. Peng, Y. Zhao, L. Sun, pH/NIR-responsive nanocarriers based on mesoporous polydopamine encapsulated gold nanorods for drug delivery and thermo-chemotherapy, J. Drug Deliv. Sci. Technol. 75 (2022) 103610, https://doi.org/10.1016/j.jddst.2022.103610.

[24] J. Huang, Z. Xu, Y. Jiang, W. Law, B. Dong, X. Zeng, M. Ma, G. Xu, J. Zou, C. Yang, Metal organic framework-coated gold nanorod as an on-demand drug delivery platform for chemo-photothermal cancer therapy, J. Nanobiotechnol. 19 (2021) 219, https://doi.org/10.1186/s12951-021-00961-x.

[25] Q. Xu, Y. Yang, J. Lu, Y. Lin, S. Feng, X. Luo, D. Di, S. Wang, Q. Zhao, Recent trends of mesoporous silica-based nanoplatforms for nanodynamic therapies, Coord. Chem. Rev. 469 (2022) 214687, https://doi.org/10.1016/j.ccr.2022.214687.

[26] Z. Liu, Z. Yan, Y. Di, S. Yang, Y. Ning, Y. Mao, Y. Gao, Q. Zhao, S. Wang, Current advances in metal–organic frameworks for cancer nanodynamic therapies, Coord. Chem. Rev. 497 (2023) 215434, https://doi.org/10.1016/j.ccr.2023.215434.

[27] N. Zhao, M. C Woodle, A.J. Mixson, Advances in delivery systems for doxorubicin, J. Nanomed. Nanotechnol. 9 (2018), https://doi.org/10.4172/2157-7439.1000519.

[28] M. Mohammadi, L. Arabi, M. Alibolandi, Doxorubicin-loaded composite nanogels for cancer treatment, J. Contr. Release 328 (2020) 171–191, https://doi.org/10.1016/j.jconrel.2020.08.033.

[29] P. Koźmiński, P.K. Halik, R. Chesori, E. Gniazdowska, Overview of dual-acting drug methotrexate in different neurological diseases, autoimmune pathologies and cancers, Int. J. Mol. Sci. 21 (2020) 3483, https://doi.org/10.3390/ijms21103483.

[30] M. Rahimi, K.D. Safa, R. Salehi, Co-delivery of doxorubicin and methotrexate by dendritic chitosan-g-mPEG as a magnetic nanocarrier for multi-drug delivery in combination chemotherapy, Polym. Chem. 8 (2017) 7333–7350, https://doi.org/10.1039/C7PY01701D.

[31] S. Karimi, H. Namazi, Targeted co-delivery of doxorubicin and methotrexate to breast cancer cells by a pH-sensitive biocompatible polymeric system based on β-cyclodextrin crosslinked glycodendrimer with magnetic ZnO core, Eur. Polym. J. 176 (2022) 111435, https://doi.org/10.1016/j.eurpolymj.2022.111435.

[32] Y. Li, S. Chen, X. Chang, F. He, R. Zhuo, Efficient Co-delivery of doxorubicin and methotrexate by pH-sensitive dual-functional nanomicelles for enhanced synergistic antitumor efficacy, ACS Appl. Bio Mater. 2 (2019) 2271–2279, https://doi.org/10.1021/acsabm.9b00230.

[33] S. Liao, W. Yue, S. Cai, Q. Tang, W. Lu, L. Huang, T. Qi, J. Liao, Improvement of gold nanorods in photothermal therapy: recent progress and perspective, Front. Pharmacol. 12 (2021), https://doi.org/10.3389/fphar.2021.664123.

[34] N. Pal, J.-H. Lee, E.-B. Cho, Recent trends in morphology-controlled synthesis and application of mesoporous silica nanoparticles, Nanomaterials 10 (2020) 2122, https://doi.org/10.3390/nano10112122.

[35] V. Pellas, D. Hu, Y. Mazouzi, Y. Mimoun, J. Blanchard, C. Guibert, M. Salmain, S. Boujday, Gold nanorods for LSPR biosensing: synthesis, coating by silica, and bioanalytical applications, Biosensors 10 (2020) 146, https://doi.org/10.3390/bios10100146.

[36] R.K. Kankala, Y. Han, J. Na, C. Lee, Z. Sun, S. Wang, T. Kimura, Y.S. Ok, Y. Yamauchi, A. Chen, K.C.-W. Wu, Nanoarchitectured structure and surface biofunctionality of mesoporous silica nanoparticles, Adv. Mater. 32 (2020), https://doi.org/10.1002/adma.201907035.

[37] X. Cui, W. Cheng, X. Han, Lipid bilayer modified gold nanorod@mesoporous silica nanoparticles for controlled drug delivery triggered by near-infrared light, J. Mater. Chem. B 6 (2018) 8078–8084, https://doi.org/10.1039/C8TB01891J.

[38] C.E. Ashley, E.C. Carnes, G.K. Phillips, D. Padilla, P.N. Durfee, P.A. Brown, T. N. Hanna, J. Liu, B. Phillips, M.B. Carter, N.J. Carroll, X. Jiang, D.R. Dunphy, C. L. Willman, D.N. Petsev, D.G. Evans, A.N. Parikh, B. Chackerian, W. Wharton, D. S. Peabody, C.J. Brinker, The targeted delivery of multicomponent cargos to cancer cells by nanoporous particle-supported lipid bilayers, Nat. Mater. 10 (2011) 389–397, https://doi.org/10.1038/nmat2992.

[39] C.A. Schütz, L. Juillerat-Jeanneret, P. Käuper, C. Wandrey, Cell response to the exposure to chitosan–TPP//alginate nanogels, Biomacromolecules 12 (2011) 4153–4161, https://doi.org/10.1021/bm201231x.

[40] A.-G. Niculescu, A.M. Grumezescu, Applications of chitosan-alginate-based nanoparticles—an up-to-date review, Nanomaterials 12 (2022) 186, https://doi.org/10.3390/nano12020186.
[41] J. Sharifi-Rad, C. Quispe, M. Butnariu, L.S. Rotariu, O. Sytar, S. Sestito, S. Rapposelli, M. Akram, M. Iqbal, A. Krishna, N.V.A. Kumar, S.S. Braga, S. M. Cardoso, K. Jafernik, H. Ekiert, N. Cruz-Martins, A. Szopa, M. Villagran, L. Mardones, M. Martorell, A.O. Docea, D. Calina, Chitosan nanoparticles as a promising tool in nanomedicine with particular emphasis on oncological treatment, Cancer Cell Int. 21 (2021) 318, https://doi.org/10.1186/s12935-021-02025-4.
[42] A.K. Mehata Vikas, M.N.L. Suseela, C. Behera, P. Kumari, S.K. Mahto, M.S. Muthu, Chitosan-alginate nanoparticles of cabazitaxel: design, dual-receptor targeting and efficacy in lung cancer model, Int. J. Biol. Macromol. 221 (2022) 874–890, https://doi.org/10.1016/j.ijbiomac.2022.09.053.
[43] H. Thai, C. Thuy Nguyen, L. Thi Thach, M. Thi Tran, H. Duc Mai, T. Thi Thu Nguyen, G. Duc Le, M. Van Can, L. Dai Tran, G. Long Bach, K. Ramadass, C. I. Sathish, Q. Van Le, Characterization of chitosan/alginate/lovastatin nanoparticles and investigation of their toxic effects in vitro and in vivo, Sci. Rep. 10 (2020) 909, https://doi.org/10.1038/s41598-020-57666-8.
[44] F.N. Sorasitthiyanukarn, C. Muangnoi, P. Rojsitthisak, P. Rojsitthisak, Chitosan-alginate nanoparticles as effective oral carriers to improve the stability, bioavailability, and cytotoxicity of curcumin diethyl disuccinate, Carbohydr. Polym. 256 (2021) 117426, https://doi.org/10.1016/j.carbpol.2020.117426.
[45] K. Yoncheva, B. Tzankov, Y. Yordanov, I. Spassova, D. Kovacheva, M. Frosini, M. Valoti, V. Tzankova, Encapsulation of doxorubicin in chitosan-alginate nanoparticles improves its stability and cytotoxicity in resistant lymphoma L5178 MDR cells, J. Drug Deliv. Sci. Technol. 59 (2020) 101870, https://doi.org/10.1016/j.jddst.2020.101870.
[46] L. Roach, S. Ye, S.C.T. Moorcroft, K. Critchley, P.L. Coletta, S.D. Evans, Morphological control of seedlessly-synthesized gold nanorods using binary surfactants, Nanotechnology 29 (2018), https://doi.org/10.1088/1361-6528/aaa99d.
[47] M. Laura Soriano, C. Carrillo-Carrion, C. Ruiz-Palomero, M. Valcárcel, Cyclodextrin-modified nanodiamond for the sensitive fluorometric determination of doxorubicin in urine based on its differential affinity towards β/γ-cyclodextrins, Microchim. Acta 185 (2018) 115, https://doi.org/10.1007/s00604-017-2660-y.
[48] M. Hroch, J. Tuková, P. Doležalová, J. Chládek, An improved high-performance liquid chromatography method for quantification of methotrexate polyglutamates in red blood cells of children with juvenile idiopathic arthritis, Biopharm. Drug Dispos. 30 (2009) 138–148, https://doi.org/10.1002/bdd.654.
[49] S. Feng, Y. Mao, X. Wang, M. Zhou, H. Lu, Q. Zhao, S. Wang, Triple stimuli-responsive ZnO quantum dots-conjugated hollow mesoporous carbon nanoplatform for NIR-induced dual model antitumor therapy, J. Colloid Interface Sci. 559 (2020) 51–64, https://doi.org/10.1016/j.jcis.2019.09.120.
[50] Q. Zhao, Y. Zhang, T. Yu, J. Lu, G. Sun, X. Luo, S. Wang, Tailored nanoplatforms with detachable 'meteorolite' for photothermal-enhanced programmed tumor therapy, Carbon N. Y. 199 (2022) 119–131, https://doi.org/10.1016/j.carbon.2022.07.073.
[51] Y. Xue, X. Ma, X. Feng, S. Roberts, G. Zhu, Y. Huang, X. Fan, J. Fan, X. Chen, Temperature-derived purification of gold nano-bipyramids for colorimetric detection of tannic acid, ACS Appl. Nano Mater. 6 (2023) 11572–11580, https://doi.org/10.1021/acsanm.3c01593.
[52] L. Vigderman, B.P. Khanal, E.R. Zubarev, Functional gold nanorods: synthesis, self-assembly, and sensing applications, Adv. Mater. 24 (2012) 4811–4841, https://doi.org/10.1002/adma.201201690.
[53] C. Wu, Q.-H. Xu, Stable and functionable mesoporous silica-coated gold nanorods as sensitive localized surface plasmon resonance (LSPR) nanosensors, Langmuir 25 (2009) 9441–9446, https://doi.org/10.1021/la900646n.
[54] H. Liu, N. Pierre-Pierre, Q. Huo, Dynamic light scattering for gold nanorod size characterization and study of nanorod–protein interactions, Gold Bull. 45 (2012) 187–195, https://doi.org/10.1007/s13404-012-0067-4.
[55] Q. Duan, M. Yang, B. Zhang, Y. Li, Y. Zhang, X. Li, J. Wang, W. Zhang, S. Sang, Gold nanoclusters modified mesoporous silica coated gold nanorods: enhanced photothermal properties and fluorescence imaging, J. Photochem. Photobiol. B Biol. 215 (2021) 112111, https://doi.org/10.1016/j.jphotobiol.2020.112111.
[56] C. Shan, Y. Huang, J. Wei, M. Chen, L. Wu, Ultra-high thermally stable gold nanorods/radial mesoporous silica and their application in enhanced chemo-photothermal therapy, RSC Adv. 11 (2021) 10416–10424, https://doi.org/10.1039/D1RA00213A.
[57] X. Wang, Y. He, X. Liu, L. Shi, J. Zhu, Investigation of photothermal heating enabled by plasmonic nanofluids for direct solar steam generation, Sol. Energy 157 (2017) 35–46, https://doi.org/10.1016/j.solener.2017.08.015.
[58] R. Hafezi Moghaddam, S. Dadfarnia, A.M.H. Shabani, Z.H. Moghaddam, M. Tavakol, Electron beam irradiation synthesis of porous and non-porous pectin based hydrogels for a tetracycline drug delivery system, Mater. Sci. Eng. C 102 (2019) 391–404, https://doi.org/10.1016/j.msec.2019.04.071.
[59] S.A.P. Siboro, D.S.B. Anugrah, K. Ramesh, S.-H. Park, H.-R. Kim, K.T. Lim, Tunable porosity of covalently crosslinked alginate-based hydrogels and its significance in drug release behavior, Carbohydr. Polym. 260 (2021) 117779, https://doi.org/10.1016/j.carbpol.2021.117779.
[60] M. Hesan, A. Gholipour-Kanani, M. Lotfi, M. Shafiee, The synthesis and characterization of core-shell nanogels based on alginate and chitosan for the controlled delivery of mupirocin, Biochem. Eng. J. 190 (2023) 108742, https://doi.org/10.1016/j.bej.2022.108742.
[61] R.R. Almeida, E.T. Silva Damasceno, S.Y.B. de Carvalho, G.S.G. de Carvalho, L.A. P. Gontijo, L.G. de Lima Guimarães, Chitosan nanogels condensed to ferulic acid for the essential oil of Lippia origanoides Kunth encapsulation, Carbohydr. Polym. 188 (2018) 268–275, https://doi.org/10.1016/j.carbpol.2018.01.103.
[62] M.M. Lakouraj, F. Mojerlou, E.N. Zare, Nanogel and superparamagnetic nanocomposite based on sodium alginate for sorption of heavy metal ions, Carbohydr. Polym. 106 (2014) 34–41, https://doi.org/10.1016/j.carbpol.2014.01.092.
[63] G. Lawrie, I. Keen, B. Drew, A. Chandler-Temple, L. Rintoul, P. Fredericks, L. Grøndahl, Interactions between alginate and chitosan biopolymers characterized using FTIR and XPS, Biomacromolecules 8 (2007) 2533–2541, https://doi.org/10.1021/bm070014y.
[64] N. Üstündağ Okur, N. Hökenek, M.E. Okur, Ş. Ayla, A. Yoltaş, P.I. Siafaka, E. Cevher, An alternative approach to wound healing field; new composite films from natural polymers for mupirocin dermal delivery, Saudi Pharm. J. 27 (2019) 738–752, https://doi.org/10.1016/j.jsps.2019.04.010.
[65] D. Pamfil, C. Vasile, Nanogels of natural polymers, in: V. Thakur, M. Thakur, S. Voicu (Eds.), Polym. Gels. Gels Horizons from Sci. To Smart Mater., Springer, Singapore, 2018, pp. 71–110, https://doi.org/10.1007/978-981-10-6080-9_4.
[66] G.S. El-Feky, S.T. El-Banna, G.S. El-Bahy, E.M. Abdelrazek, M. Kamal, Alginate coated chitosan nanogel for the controlled topical delivery of Silver sulfadiazine, Carbohydr. Polym. 177 (2017) 194–202, https://doi.org/10.1016/j.carbpol.2017.08.104.
[67] M. Danaei, M. Dehghankhold, S. Ataei, F. Hasanzadeh Davarani, R. Javanmard, A. Dokhani, S. Khorasani, M.R. Mozafari, Impact of particle size and polydispersity index on the clinical applications of lipidic nanocarrier systems, Pharmaceutics 10 (2018) 57, https://doi.org/10.3390/pharmaceutics10020057.
[68] K. Yoncheva, M. Merino, A. Shenol, N.T. Daskalov, P. St Petkov, G.N. Vayssilov, M. J. Garrido, Optimization and in-vitro/in-vivo evaluation of doxorubicin-loaded chitosan-alginate nanoparticles using a melanoma mouse model, Int. J. Pharm. 556 (2019) 1–8, https://doi.org/10.1016/j.ijpharm.2018.11.070.
[69] V. Huber, C. Camisaschi, A. Berzi, S. Ferro, L. Lugini, T. Triulzi, A. Tuccitto, E. Tagliabue, C. Castelli, L. Rivoltini, Cancer acidity: an ultimate frontier of tumor immune escape and a novel target of immunomodulation, Semin. Cancer Biol. 43 (2017) 74–89, https://doi.org/10.1016/j.semcancer.2017.03.001.
[70] G. Hao, Z.P. Xu, L. Li, Manipulating extracellular tumour pH: an effective target for cancer therapy, RSC Adv. 8 (2018) 22182–22192, https://doi.org/10.1039/C8RA02095G.
[71] J. Nan, Y. Chen, R. Li, J. Wang, M. Liu, C. Wang, F. Chu, Polymeric hydrogel nanocapsules: a thermo and pH dual-responsive carrier for sustained drug release, Nano-Micro Lett. 6 (2014) 200–208, https://doi.org/10.1007/BF03353784.
[72] Q.-S. Wang, L.-N. Gao, X.-N. Zhu, Y. Zhang, C.-N. Zhang, D. Xu, Y.-L. Cui, Co-delivery of glycyrrhizin and doxorubicin by alginate nanogel particles attenuates the activation of macrophage and enhances the therapeutic efficacy for hepatocellular carcinoma, Theranostics 9 (2019) 6239–6255, https://doi.org/10.7150/thno.35972.
[73] N.S. Elbialy, N. Mohamed, Alginate-coated caseinate nanoparticles for doxorubicin delivery: preparation, characterisation, and in vivo assessment, Int. J. Biol. Macromol. 154 (2020) 114–122, https://doi.org/10.1016/j.ijbiomac.2020.03.027.
[74] S.R.S. Veloso, E. Tiryaki, C. Spuch, L. Hilliou, C.O. Amorim, V.S. Amaral, P.J. G. Coutinho, P.M.T. Ferreira, V. Salgueiriño, M.A. Correa-Duarte, E.M. S. Castanheira, Tuning the drug multimodal release through a co-assembly strategy based on magnetic gels, Nanoscale 14 (2022) 5488–5500, https://doi.org/10.1039/D1NR08158F.
[75] L. Yang, J. Ling, N. Wang, Y. Jiang, Y. Lu, L.-Y. Yang, X. Ouyang, Delivery of doxorubicin by dual responsive carboxymethyl chitosan based nanogel and in vitro performance, Mater. Today Commun. 31 (2022) 103781, https://doi.org/10.1016/j.mtcomm.2022.103781.
[76] A. Alioghli Ziaei, H. Erfan-Niya, M. Fathi, N. Amiryaghoubi, In situ forming alginate/gelatin hybrid hydrogels containing doxorubicin loaded chitosan/AuNPs nanogels for the local therapy of breast cancer, Int. J. Biol. Macromol. 246 (2023) 125640, https://doi.org/10.1016/j.ijbiomac.2023.125640.
[77] M. Meloun, Z. Ferenčíková, A. Vrána, The thermodynamic dissociation constants of methotrexate by the nonlinear regression and factor analysis of multiwavelength spectrophotometric pH-titration data, Open Chem. 8 (2010) 494–507, https://doi.org/10.2478/s11532-010-0023-1.
[78] M. Mohammed, J. Syeda, K. Wasan, E. Wasan, An overview of chitosan nanoparticles and its application in non-parenteral drug delivery, Pharmaceutics 9 (2017) 53, https://doi.org/10.3390/pharmaceutics9040053.
[79] F. Karami, S. Ranjbar, Y. Ghasemi, M. Negahdaripour, Analytical methodologies for determination of methotrexate and its metabolites in pharmaceutical, biological and environmental samples, J. Pharm. Anal. 9 (2019) 373–391, https://doi.org/10.1016/j.jpha.2019.06.001.
[80] K.M. Hamed, I.M. Dighriri, A.F. Baomar, B.T. Alharthy, F.E. Alenazi, G.H. Alali, R. H. Alenazy, N.T. Alhumaidi, D.H. Alhulayfi, Y.B. Alotaibi, S.S. Alhumaidan, Z. A. Alhaddad, A.A. Humadi, S.A. Alzahrani, R.H. Alobaid, Overview of methotrexate toxicity: a comprehensive literature review, Cureus (2022), https://doi.org/10.7759/cureus.29518.
[81] J. Wang, Z. Zhang, Y. Ai, F. Liu, M.-M. Chen, D. Liu, Lactobionic acid-modified thymine-chitosan nanoparticles as potential carriers for methotrexate delivery, Carbohydr. Res. 501 (2021) 108275, https://doi.org/10.1016/j.carres.2021.108275.
[82] Y. Sheng, C. Cao, Z. Liang, Z.-Z. Yin, J. Gao, W. Cai, Y. Kong, Construction of a dual-drug delivery system based on oxidized alginate and carboxymethyl chitosan for chemo-photothermal synergistic therapy of osteosarcoma, Eur. Polym. J. 174 (2022) 111331, https://doi.org/10.1016/j.eurpolymj.2022.111331.
[83] P. Nezhad-Mokhtari, M. Ghorbani, F. Mahmoodzadeh, Smart co-delivery of 6-mercaptopurine and methotrexate using disulphide-based PEGylated-nanogels for

effective treatment of breast cancer, New J. Chem. 43 (2019) 12159–12167, https://doi.org/10.1039/C9NJ02470K.
[84] H. Chen, Y. Sun, X. Xu, Q. Ye, Targeted delivery of methotrexate by modified yeast β-glucan nanoparticles for rheumatoid arthritis therapy, Carbohydr. Polym. 284 (2022) 119183, https://doi.org/10.1016/j.carbpol.2022.119183.
[85] M.R. Rajeev, V. Manjusha, T.S. Anirudhan, Transdermal delivery of doxorubicin and methotrexate from polyelectrolyte three layer nanoparticle of graphene oxide/polyethyleneimine/dextran sulphate for chemotherapy: in vitro and in vivo studies, Chem. Eng. J. 466 (2023) 143244, https://doi.org/10.1016/j.cej.2023.143244.
[86] S. Dash, P.N. Murthy, L. Nath, P. Chowdhury, Kinetic modeling on drug release from controlled drug delivery systems, Acta Pol. Pharm. - Drug Res. 67 (2010) 217–223.
[87] P.L. Ritger, N.A. Peppas, A simple equation for description of solute release II. Fickian and anomalous release from swellable devices, J. Contr. Release 5 (1987) 37–42, https://doi.org/10.1016/0168-3659(87)90035-6.
[88] J. Bergueiro, E.A. Glitscher, M. Calderón, A hybrid thermoresponsive plasmonic nanogel designed for NIR-mediated chemotherapy, Biomater. Adv. 137 (2022) 212842, https://doi.org/10.1016/j.bioadv.2022.212842.